Co-precipitation Synthesis and Photocatalytic Activity of Mn-doped SrTiO_3 for the Degradation of Methylene Blue Wastewater

Iriani, Yofentina
Department of Physics, Faculty of Mathematics and Natural Science, Universitas Sebelas Maret

Afriani, Rindhi
Department of Physics, Faculty of Mathematics and Natural Science, Universitas Sebelas Maret

Dianisa Khoirum Sandi
Department of Physics, Faculty of Mathematics and Natural Science, Universitas Sebelas Maret

Nurosyid, Fahru
Department of Physics, Faculty of Mathematics and Natural Science, Universitas Sebelas Maret

https://doi.org/10.5109/6625717

Co-precipitation Synthesis and Photocatalytic Activity of Mn-doped SrTiO₃ for the Degradation of Methylene Blue Wastewater

Yofentina Iriani[*], Rindhi Afriani, Dianisa Khoirum Sandi, Fahru Nurosyid

Department of Physics, Faculty of Mathematics and Natural Science, Universitas Sebelas Maret, Indonesia

*Author to whom correspondence should be addressed:
E-mail: yofent_iriani@staff.uns.ac.id

Abstract: Wastewater has been one of the major issues concerned by researchers in developing countries such as Indonesia. The wastewater contaminants can be removed by a photocatalytic process using a photocatalyst material, and one famous is Strontium Titanate (SrTiO₃ or STO). STO doped with metals, one of which is Manganese (Mn), can improve its photocatalytic activity. Synthesis of Mn-doped STO ($SrTi_{1-x}Mn_xO_3$, where x=0.05-0.2) has been completed via the co-precipitation method to examine the influences of Mn concentrations on the microstructure, chemical bonds, and photocatalytic activity of STO material. The characterization employed X-Ray Diffraction (XRD), Fourier Transform Infra-Red (FTIR), and UV-Vis spectrophotometer. The data revealed that Mn-doped STO samples had been formed with high crystallinity. The photocatalytic activity of the Mn-doped STO samples was examined with the degradation of 10 ppm methylene blue (MB) under UV irradiation. The yields demonstrated that all samples have successfully become photocatalysts by degrading MB. The degradation was affected by the crystallinity and surface area of the samples. The study found that the best Mn-doped STO resulting in 54.69% MB degradation was from x=0.15 with 5 hours irradiation.

Keywords: Strontium Titanate (STO), Manganese (Mn), Mn-doped STO, photocatalyst, methylene blue (MB), degradation

1. Introduction

Water contamination in Indonesia has become the most concerned issue among Indonesian researchers today. 3,7-bis (Dimethylamine)-phenothiazine-5-ium chloride or Methylene Blue (MB), which is the common dye highly used in plastic, paper, pharmaceutical, cotton, leather, and textile industries, is one of the primary pollutants of water contamination[1,2]. MB wastewater thrown into the environment is extremely hazardous to human and aquatic life[3]. To deal with this issue, it is crucial to degrade this MB wastewater in the environment. One of the most favorable approaches that are currently being developed is heterogeneous photocatalysis[4]. It is a process of degrading harmful materials to less harmful and less toxic materials by illuminating them with sunlight or other irradiation sources, such as ultraviolet, microwave, etc[5]. The photocatalyst material for heterogeneous photocatalysis approaches that is being extensively studied currently is Strontium Titanate (SrTiO₃ or STO).

Considering its future application, STO is one of the most crucial oxide materials. STO includes perovskite material with ABO₃ cubic crystal structure, 3.9046 Å lattice constant (a), and Pm3m space group[4, 6, 7]. It has bandgap energy and a density of 3.2 eV and 5.18 g/cm³ at surrounding temperatures[8]. STO has remarkable physical and chemical features, including high thermal and chemical stability, dielectric, nonlinear optic coefficient, paraelectricity, superconductivity, and photocatalytic activity[8-10]. Based on the features, STO is prospective to be developed sustainably in many applications. Several applications that utilize STO as the main material are photocatalysts, capacitors, sensors, and other optoelectronic devices[7, 11-13].

In recent years, many studies have been conducted regarding doping STO with transition metals such as Rh, Ru, Ag, Y, Cd, Ni, Cr, and Mn, showing the improvement in the photocatalytic activity of STO[4, 11, 14-20]. Compared to the existing dopants, Mn is desirable for doping STO. It is due to the ionic radius of Mn⁴⁺ (0.67 Å) which is close to Ti⁴⁺ ionic radius (0.68 Å), and their same coordinate number of 6[4, 18]. Thus, the inclusion of the Mn atom can easily replace the Ti atom in the structure crystal so that it can decline the conduction band and narrow the bandgap energy[4, 18]. It has been reported by many researchers regarding the wide bandgap of STO (> 3.2 eV) that makes STO photocatalyst only be used under UV irradiation.

Therefore, STO as a photocatalyst is expected to be more applicable to real-life through doping.

Several methods commonly employed to synthesize STO are hydrothermal[21], sol-gel[19], solid-state reaction[22,23], and coprecipitation. Among the methods, the co-precipitation method is chosen because it is relatively inexpensive and straightforward[24,25]. Besides, the method has good homogeneity and stoichiometry control[24,26]. This method incorporates two or more different materials in solid or liquid. To the best of our knowledge, using this method, the synthesis of -doped STO as a photocatalyst, especially with Mn dopant, is rarely found.

Hence, in this context, this study focused on synthesizing STO material doped with various concentrations of Mn ($SrTi_{1-x}Mn_xO_3$ where x=0.05, 0.01, 0.15, and 0.20) using the co-precipitation method. Further, this study purposed to examine the influences of varied Mn concentrations on the microstructure, chemical bonds, and the performance of STO as the photocatalyst material.

2. Method

2.1 Materials

The main ingredients were Strontium Nitrate [$Sr(NO_3)_2$], Titanium Tetrabutoxide [$Ti(OCH_2CH_2CH_3)_4$] (Sigma Aldrich, 97%), Oxalic Acid Dihydrate [$C_2H_2O_4.2H_2O$] (Merck $\geq$ 99%), Manganese (II) Nitrate Tetrahydrate [$Mn(NO_3)_2.4H_2O$] (Merck), and Isopropanol (IPA).

2.2 Synthesis of Mn-doped STO ($SrTi_{1-x}Mn_xO_3$)

Mn-doped STO samples were prepared using the co-precipitation method. First, the ingredients were weighed according to the stoichiometry formula of $SrTi_{1-x}Mn_xO_3$, where x is the Mn concentrations varied by 0.05, 0.10, 0.15, and 0.20. Next, Oxalic Acid Dihydrate was dissolved in IPA by stirring (later called Solution A). After that, Strontium Nitrate and IPA were added to Solution A and stirred (later called Solution B). Titanium Tetrabutoxide was dissolved in IPA (later called Solution C). After that, Manganese (II) Nitrate Tetrahydrate and Solution C were mixed and then added to Solution B by stirring. Then titration was performed on the resulting solution with distilled water. It was then precipitated for 24 hours. Afterward, the hydrolyzation process was done on the samples by heating them at 100ºC for 10 hours in an oven. The dried samples were sintered at a temperature of 1000ºC for 4 hours. The resulting samples are labeled STO: Mn5, STO: Mn10, STO: Mn15, and STO: Mn20 standing for the Mn concentrations (x) of 0.05, 0.1, 0.15, and 0.20, respectively. Finally, the samples were examined via X-Ray Diffraction (XRD), Fourier Transform Infra-Red (FTIR), and photocatalytic activity testing.

2.3 XRD Characterization

Characterization by means of XRD was to determine the crystal structure of Mn-doped STO samples. The diffraction pattern produced from XRD characterization was matched with the ICDD database and refined by Rietveld analysis using GSAS software. It was then used to calculate the crystallite size (Equation 1 and Equation 6), lattice constants, crystallization level (Equation 7), and lattice strain (Equation 8). The crystallite size of the samples was computed through the Scherrer equation and the Williamson Hall method (WH Plot) as Equation 1 and Equation 2-6, respectively[27].

$$D = k\lambda/ \beta \cos\theta \qquad (1)$$

Where β, θ, k, λ, D, and ε are the FWHM value (rad), X-ray diffraction angle (degrees), Scherrer constant (0.94), X-ray wavelength (nm), crystallite size (nm), and lattice strain, respectively. Meanwhile, the WH Plot method is written as follows.

$$\beta_D = [\beta_{measured}^2 - \beta_{instrumental}^2] \qquad (2)$$

$$D = k\lambda/ \beta \cos\theta \rightarrow \cos\theta = k\lambda/ D\beta \quad (3)$$

$$\beta_{hkl} = \beta_s + \beta_D \qquad (4)$$

$$\beta_{hkl} = k\lambda/ D \cos\theta + 4\varepsilon \tan\theta \qquad (5)$$

$$\beta_{hkl} \cos\theta = k\lambda/ D + 4\varepsilon \sin\theta \qquad (6)$$

The degree of crystallinity of Mn-doped STO can be determined using the following equation[28].

$$Crystallinity\ \% = \frac{intensity_{max}}{intensity_{max}+intensity_{min}}\ x\ 100\% \quad (7)$$

Lattice strain (ε) samples can be calculated using the following equation[27,28].

$$\varepsilon = \beta_D/ 4\tan\theta \qquad (8)$$

2.4 FTIR Characterizations

The characterization of Mn-doped STO with FTIR was to specify the chemical bonds of the samples. The observation was made in $400 – 4000\ cm^{-1}$ wavenumbers.

2.5 Photocatalyst activity

The photocatalyst activity of the Mn-doped STO was assessed with the degradation of 10 ppm methylene blue (MB) under UV irradiation. It was carried out by adding 0.01 g of Mn-doped STO sample in 10 ml of 10 ppm MB solution. The solution was left for 24 h in a dark condition for the adsorption-desorption equilibrium. Then it is put in a set of UV tools and stirred while irradiating with a UV lamp (λ= 320 – 290 nm). The irradiation times were varied by 4 and 5 hours. After being irradiated, the solution was left for 24 hours in the dark. Furthermore, the

photocatalyst samples were tested by means of a UV-Vis spectrophotometer to find the absorbance value and the level (%) of MB degradation. The % MB degradation was calculated using Equation 9 as follows. Where A_o is the initial absorbance and A_t is the absorbance after time t.

$$DR\% = (A_o - A_t)/Ao \; x100\% \qquad (9)$$

3. Results and discussion

Mn-doped STO samples have been successfully formed using the co-precipitation method with mole concentrations of Mn doping (x = 5%, 10%, 15%, and 20%). The microstructure investigation of Mn-doped STO samples was carried out using XRD. The results of the Mn-doped STO are diffractograms exposed in Fig. 1(a). The diffractograms were appropriate with ICDD PDF database #860178, confirming that the peaks correspond to the SrTiO₃ phase. These results also exhibit that the sample has a cubic crystal structure with a *Pm3m* space group. Based on Fig. 1(a), other peaks or impurity phases are marked (*) and identified as the SrCO₃ phase. This impurity is associated with carbonates formed if hydroxide or SrO interacts with CO_2 during the reaction[18]. However, this impurity vanishes at the highest Mn dopant concentration (0.2), indicating that doping promotes the reaction entirely. The absence of the MnO peak signifies the successful insertion of Mn into the SrTiO₃ lattice.
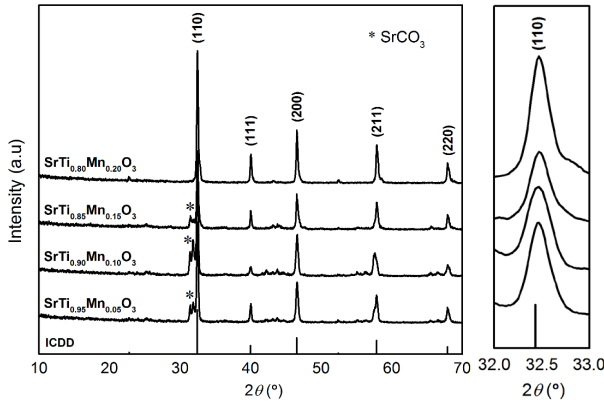

Fig. 1: (left) Diffractograms of Mn-doped STO samples and (right) magnification of the prominent (110) peaks of samples

Table 1. Lattice constants from the calculation and Rietveld Refinement process

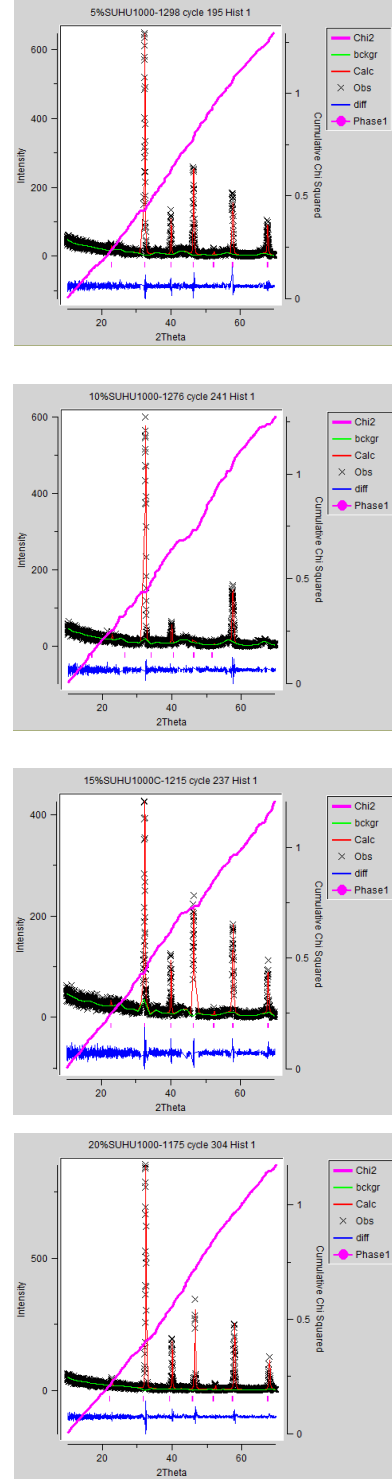| Samples	Lattice parameters (Å)	
	Calculation	Rietveld Refinement Process
STO: Mn5	3.8975	3.9104
STO: Mn10	3.8977	3.9417
STO: Mn15	3.8973	3.9105
STO: Mn20	3.8970	3.8953

Fig. 2: Refinement results of the samples (a) STO: Mn5, (b) STO: Mn10, (c) STO: Mn15, (d) STO: Mn20

Likewise, Fig. 1(b) presents the variations in the moles' concentration of Mn doping, causing a right shift in the diffraction angle (2θ). The shift could be attributed to the slight distinctions of ionic radius between Mn^{4+} and Ti^{4+} that denote the changes in the lattice constant of the samples, as shown in Table 1. Both suggest that Mn ions have been doped into the STO host structure corresponding crystal sites. A similar occurrence has also

occurred in other literature, for instance, the Mn-doped STO fabricated by Wu et al. [4]. Moreover, with doping of Mn, the intensity of diffraction peaks increases, and the width of the peaks also narrows. The increment of peak intensities and narrowing might be related to the enlargement of the crystallite size and reduction in the lattice strain stimulated by Mn substitution [29], as shown in Fig. 3 and Table 2, respectively. Furthermore, the sharp and narrow XRD peaks denote that all samples are nanocrystals with high quality and good crystallinity [28, 29], as illustrated in Fig. 3 and Table 2.

Table 1 presents the lattice constants of the samples obtained from the calculation and refinement process by Rietveld analysis using GSAS software. The refinement results are displayed in Fig. 2. The green color in the graph is the background of the histogram, the cross is the observed data or the XRD data, the red color is the calculated data of the refinement data from GSAS, and the blue color shows the distinction between the observed and calculated data. The GSAS processing is done through background refinement to approximate the calculated curves close to the observed curves. So that a small Chi2 value (less than 2) is obtained until convergence is formed.
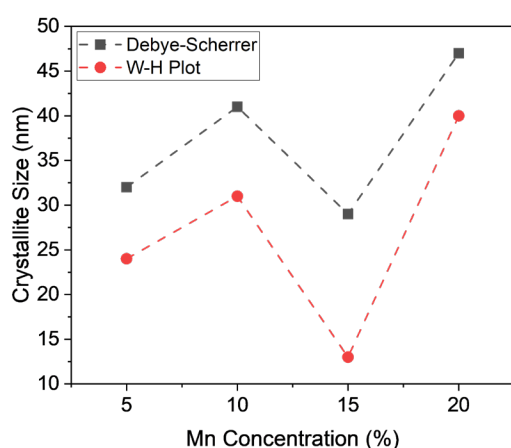

Fig. 3: The crystallite size of Mn-doped STO by Debye-Scherrer and WH Plot methods

Table 2. Crystallinity level and lattice strain of Mn-doped STO samples

Sample	Crystallinity (%)	Lattice Strain
STO: Mn 5	96.58	0.0027
STO: Mn 10	97.09	0.0027
STO: Mn 15	96.36	0.0021
STO: Mn 20	97.15	0.0021

The lattice constants calculated by the Rietveld Refinement process are shown in Table 2. Both results demonstrate that a linear correlation between the addition of Mn concentrations and the lattice constants is not achieved in this study. The lattice constants exhibit an increment from Mn concentrations of 5% to 10% and then a decrement from 10% to 20%. It might be due to Mn acting as Mn^{4+} and the others as Mn^{2+} that either replace

Sr^{2+} site or Ti^{4+} site where the ionic radius of Mn^{2+} (0.82 Å) is much smaller than Sr^{2+} (1.12 Å) and the ionic radius of Mn^{4+} (0.67 Å) is slightly smaller than Ti^{4+} (0.68 Å).

Fig. 3 shows the crystallite size of Mn-doped STO calculated using the Debye-Scherrer (Equation 1) and the WH Plot method (Equation 2-6). The crystallite size of STO: Mn5, STO: Mn10, STO: Mn15, and STO: Mn20, using the Debye-Scherrer, are 32, 41, 29, and 47 nm, respectively. Meanwhile, with the WH Plot method, the crystallite sizes are 24, 31, 13, and 40 nm for STO: Mn5, STO: Mn10, STO: Mn15, and STO: Mn20, respectively. Similarly, it is seen that using these two methods, linear crystallite size values of the Mn-doped STO samples could not be obtained as the mole concentration of Mn doping increases. While the lattice strain declines with Mn doping, as written in Table 2. The decline in the lattice strain implies a reduction in lattice imperfections, which indicates the formation of a better quality of the samples as the more Mn dopant addition[28].

The chemical bonds of the Mn-doped STO samples were characterized using FTIR, as shown in Fig. 4. The FTIR spectra of the samples were estimated and observed in the wavenumber range of 400-4000 cm^{-1}. Fig. 4 shows that there is a strong absorption band in the wave numbers range of 560.35-565.17 cm^{-1} and 1454.39-1459.21 cm^{-1}. These results follow the study done by Jarabana et al.[22]. The wavenumber range of 560.35-565.17 cm^{-1} points to Sr-Ti-O stretching. The appearance of Sr-Ti-O stretching indicated that the Mn-doped STO sample was successfully fabricated. While in the wavenumber range of 1454.39-1459.21 cm^{-1} reveals the existence of CH bending. Another absorption band is in the wavenumbers area of 860.29 – 861.25 cm^{-1} denoting the presence of OH stretching[19], which is recognized to the H_2O molecules presented in the samples. Meanwhile, Mn-O vibrational bonds were not detected at 620 cm^{-1} wavenumbers[16]. This indicates that the Mn doping successfully enters the $SrTiO_3$ crystal lattice. This result is supported by XRD data analysis which shows that the absence of MnO peaks suggests the insertion of Mn into the crystal lattice of $SrTiO_3$.
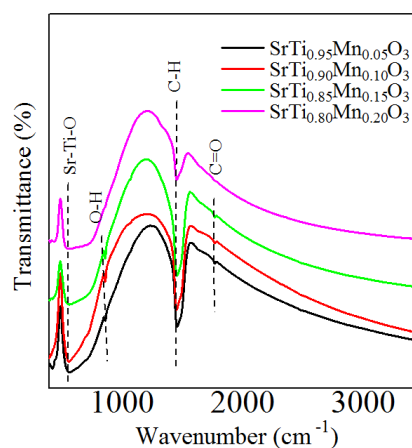

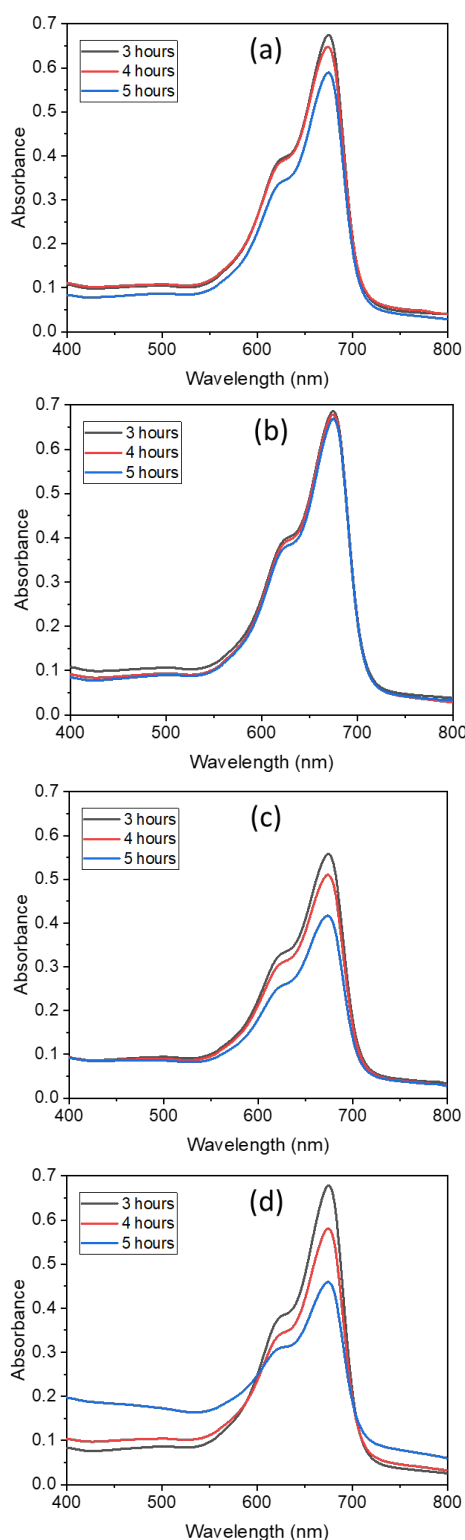**Fig. 4:** FTIR spectra of Mn-doped STO samples

Fig. 5: The results of the UV-Vis spectrophotometer characterization at 4 and 5 hours of UV irradiation (a) STO: Mn5, (b) STO: Mn10, (c) STO: Mn15, (d) STO: Mn20

The photocatalytic activity of the Mn-doped STO samples was shown by the methylene blue (MB) dye degradation under UV irradiation. Fig. 5 displays the absorbance value of MB solution after UV irradiation for 3, 4, and 5 hours. Based on Fig. 5, the absorbance value of MB decreases with increasing irradiation time. This implies that the MB solution has been decayed by Mn-doped STO photocatalysts under UV irradiation[30]. Besides, it also means that the photocatalytic process occurs in all samples of Mn-doped STO. It also demonstrates that MB was degraded more effectively by Mn-doped STO under UV irradiation for a longer time. It is attributed to the photocatalytic degradation kinetics during the irradiation process. The longer irradiation times cause more dye molecules to be irradiated. It drives higher photocatalytic degradation and photoreaction, so more MB particles are degraded, demonstrated by decreasing absorbance values.

Furthermore, the percentage value of MB degradation by the Mn-doped STO samples can be obtained from the absorbance value, as presented in Fig. 6. According to the figure, the percentage of MB degradation ups and downs as the Mn concentration increases. Numerous aspects influence the activity of a photocatalyst, namely the crystallinity, crystal phase, particle size, surface area, and others that can be modified based on heat treatments or added materials or doping[2,31].
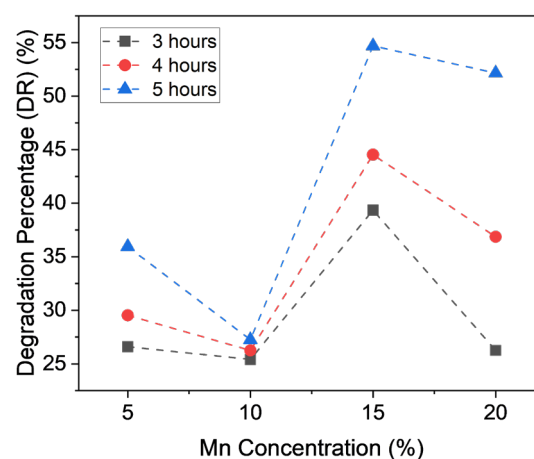

Fig 6: Degradation percentage (*DR*%) of 10 ppm MB with the variation of Mn dopant concentration at 3, 4, and 5 hours UV irradiation

Based on the XRD results, all samples possess high crystallinity. If seen, the trend is inversely proportional to the crystallite size of the samples. From Fig. 3 and Fig. 6, using the Debye Scherrer method and at 4 hours of UV irradiation, the crystallite size and degradation percentage of the STO: Mn5 are 32 nm and 29.53%, then at the STO: Mn10 sample, they are 41 nm and 26.29 %, while at the STO: Mn15 and STO: Mn20 samples are 29 nm and 44.53%; and 47 nm and 36.38%, respectively. At 3 hours of irradiation, the degradation percentages are 26.6% (STO: Mn5), 25.41% (STO: Mn10), 39.35% (STO: Mn15), and 26.25% (STO: Mn15). Meanwhile, the degradation percentages for 5 hours of irradiation are 35.94% (STO: Mn5), 27.26% (STO: Mn10), 54.69% (STO: Mn15), and 52.15% (STO: Mn20). When the crystallite size decreases, the degradation percentage increases, and vice versa. The photocatalytic activity of

Mn-doped STO under UV irradiation is associated with crystallinity and crystallite size. Crystallinity and crystallite size have a role in controlling the migration of charge carriers to the catalyst surface, thus reducing electron-hole recombination and increasing the degradation percentage. Overall, the highest MB degradation percentage was achieved by the STO: Mn15 sample at 5 hours of UV irradiation.

4. Conclusion

Mn-doped STO samples have been prepared via the co-precipitation method with various Mn mole concentrations (x) of 5%, 10%, 15%, and 20%. XRD and FTIR results denote that the Mn-doped STO samples have been successfully prepared. The photocatalytic activity showed that the Mn-doped STO samples have succeeded in becoming a photocatalyst by degrading MB under UV irradiation. Further, the degradation percentage showed that a longer irradiation time resulted in a higher degradation percentage. The degradation was influenced by the crystallinity and crystallite size. This study exhibited that the best mole concentration of doping and the irradiation time to produce Mn-doped STO photocatalyst were x=0.15 and 5 hours, which could achieve a degradation percentage of 54.69%.

Acknowledgments

References

1) K. Maniammala, G. Madhu, and V. Bijua, "Nanostructured mesoporous NiO as an efficient photocatalyst for degradation of methylene blue: structure, properties and performance," *Nano-Structures & Nano-Objects*, 16(4) 266-275 (2018). https://doi.org/10.1016/j.nanoso.2018.07.007

2) N. I. I. Zamri, S. L. N. Zulmajdi, E. Kusrini, K. Ayuningtyas, H. M. Yasin, and A. Usman, "Rhodamine B Photocatalytic Degradation using CuO Particles under UV Light Irradiation for Applications in Industrial and Medical Fields," *EVERGREEN Joint Journal of Novel Carbon Resource Sciences & Green Asia Strategy*, 7(2), 280-284 (2020).

3) M. Ezaki and K. Kusakabe, "Highly Crystallized Tungsten Trioxide Loaded Titania Composites prepared by Using Ionic Liquids and their Photocatalytic Behaviors," *EVERGREEN Joint Journal of Novel Carbon Resource Sciences & Green Asia Strategy*, 1(02), 18-24 (2014)

4) G. Wu, P. Li, D. Xu, B. Luo, Y. Hong, W. Shi, and C. Liu, "Hydrothermal synthesis and visible-light-driven photocatalytic degradation for tetracycline of Mn-doped $SrTiO_3$ nanocubes," *Applied Surface Science*, 333 39-47 (2015). http://dx.doi.org/10.1016/j.apsusc.2015.02.008

5) D. Ali, M. Z. Butt, I. Muneer, M. A. Farrukh, M. Aftab, M. Saleem, F. Bashir, and AU. Khan, "Synthesis and characterization of sol-gel derived La and Sm doped ZnO thin films: A solar light photo catalyst for methylene blue," *Thin Solid Films,* 679 86-98 (2019). https://doi.org/10.1016/j.tsf.2019.04.017

6) M. Klusáčková, R. Nebel, K. M. Macounová, M. Klementová, and P. Krtil, "Size control of the photo-electrochemical water splitting activity of $SrTiO_3$ nano-cubes," *Electrochimica Acta,* 297 215-222 (2019). https://doi.org/10.1016/j.electacta.2018.11.185

7) X. L. Shi, H. Wua, Q. Liu, W. Zhou, S. Lu, Z. Shao, M. Dargusch, and Z. G. Chen, "$SrTiO_3$-based thermoelectrics: Progress and challenges," *Nano Energy,* 78 105195 (2020). https://doi.org/10.1016/j.nanoen.2020.105195

8) S. Patial, V. Hasija, P. Raizada, P. Singh, A. A. P. K. Singh, and A. M. Asiri, "Tunable photocatalytic activity of $SrTiO_3$ for water splitting: Strategies and future scenario *Journal of Environmental Chemical Engineering*, 8(3) (2020). https://doi.org/10.1016/j.jece.2020.103791

9) F. Gao, S. Yang, J. Li, M. Qin, Y. Zhang, and H. Sun, "Fabrication, dielectric, and thermoelectric properties of textured $SrTiO_3$ ceramics prepared by RTGG method," *Ceramics International,* 41(1) 127-135 (2015). http://dx.doi.org/10.1016/j.ceramint.2014.08.045

10) H. Gao, H. Yang, and S. Wang, "Hydrothermal synthesis, growth mechanism, optical properties and photocatalytic activity of cubic $SrTiO_3$ particles for the degradation of cationic and anionic dyes," *Optik,* 175 237-249 (2018). https://doi.org/10.1016/j.ijleo.2018.09.027

11) R. Han, M. A. Melo Jr, Z. Zhao, Z. Wu, and F. E. Osterloh, "Light Intensity Dependence of Photochemical Charge Separation in the $BiVO_4$/Ru-$SrTiO_3$:Rh Direct Contact Tandem Photocatalyst for Overall Water Splitting," *The Journal of Physical Chemistry C,* 124(18) 9724-9733 (2020).

12) Z. Tian-Fu, T. Xin-Gui, H. Xian-Xiong, L. Qiu-Xiang, J. Yan-Ping, and Z. Qi-Fa, "High-Temperature Dielectric Relaxation Behaviors of Relaxer-Like $PbZrO_3$-$SrTiO_3$ Ceramics for Energy-Storage Applications," *Energy Technology,* 4(5) 633-640 (2016). DOI 10.1002/ente.201500436

13) H. P. Duong, T. Mashiyama, M. Kobayashi, A. Iwase, A. Kudo, Y. Asakura, S. Yin, M. Kakihana, and H. Katoa, "Z-scheme water splitting by microspherical Rh-doped $SrTiO_3$ photocatalysts prepared by a spray

drying method," *Applied Catalysis B: Environmental,* **252** 222-229 (2019). https://doi.org/10.1016/j.apcatb. 2019.04.009

14) Z. Liu, and Z. Ma, "Ag-SrTiO₃/TiO₂ composite nanostructures with enhanced photocatalytic activity," *Materials Research Bulletin,* **118** (2019). https://doi. org/10.1016/j.materresbull.2019.110492

15) M. Xiaoqing, X. Cui, Z. Zhao, M. A. Melo, E. J. Roberts, and F. E. Osterloh, "Use of surface photovoltage spectroscopy to probe energy levels and charge carrier dynamics in transition metal (Ni, Cu, Fe, Mn, Rh) doped SrTiO₃ photocatalysts for H₂ evolution from water," *Journal of Materials Chemistry A,* **6**(14) 5774-5781 (2018). DOI: 10.1039/ C7TA10934B

16) C. Macías-Sotelo, A. Cruz-López, and S. I. Suárez-Vázquez, "SrTi$_{1-X}$Mn$_X$O₃ and MnO$_X$/SrTiO₃ with dendritic morphology: A comparison of physico-chemical properties and soot catalytic combustion," *Materials Chemistry and Physics,* **228** 194-200 (2019). https://doi.org/10.1016/j.matchemphys.2019.02.055

17) E. Padmini, and K. Ramachandran, "Investigation on versatile behaviour of Cd doped SrTiO₃ perovskite structured compounds," *Solid State Communications,* **302** 113716 (2019). https://doi.org/10.1016/j.ssc. 2019.113716

18) S. I. Suárez-Vázquez, A. Cruz-López, C. E. Molina-Guerrero, A. I. Sánchez-Vázquez, and C. Macías-Sotelo, "Effect of Dopant Loading on the Structural and Catalytic Properties of Mn-Doped SrTiO₃ Catalysts for Catalytic Soot Combustion," *Catalysts,* **8**(2) 71 (2018). doi:10.3390/catal8020071

19) T. Xie, Y. Wang, C. Liu, and L. Xu, "New Insights into Sensitization Mechanism of the Doped Ce (IV) into Strontium Titanate," *Materials (Basel),* **11**(4) 646 (2018). doi:10.3390/ma11040646

20) D. Yang, X. Zhao, X. Zou, Z. Zhou, and Z. Jiang, "Removing Cr (VI) in water via visible-light photocatalytic reduction over Cr-doped SrTiO₃ nanoplates," *Chemosphere,* **215** 586-595 (2019). DOI: 10.1016/j.chemosphere.2018.10.068

21) F. Pellegrino, F. Sordello, L. Mino, M. Prozzi, U. Mansfeld, V. Hodoroaba, and C. Minero, "Polyethylene Glycol as Shape and Size Controller for the Hydrothermal Synthesis of SrTiO₃ Cubes and Polyhedra," *Nanomaterials (Basel),* **10**(9) 1892 (2020). doi:10.3390/nano10091892

22) K. M. Jarabana, A. Mishra, and S. Bisen, "Structural and Optical properties of poly-crystalline BaTiO₃ and SrTiO₃ prepared via solid state route," *Journal of Physics: Conference Series,* **755** 012020 (2016). doi:10.1088/1742-6596/755/1/012020

23) H. Trabelsi, M. Bejar, E. Dhahri, M. Sajieddine, K. Khirouni, P.R. Prezas, B. M. G. Melo, M. A. Valente, and M. P. F. Graça, "Effect of oxygen vacancies on SrTiO₃ electrical properties," *Journal of Alloys and Compounds,* **723** 894-903 (2017). http://dx.doi.org/ 10.1016/j.jallcom.2017.06.313

24) U. Ulfa, Y. Iriani, and K. Kusumandari, "Microstructure, Morphology, and Dielectric Properties of Ba$_{1-x}$La$_x$TiO₃ with Variation Mole Concentration of Lanthanum by Coprecipitation Method," *IOP Conference Series: Materials Science and Engineering,* 1096(1) (2017).

25) D. N. Hikmah, D. K. Sandi, F. Nurosyid, and Y. Iriani, "Effects of Sintering Temperature and Holding Times on the Microstructure and Chemical Bond of Strontium Titanate (SrTiO₃)," *Journal of Physics: Conference Series,* **2110**(1) 012011 (2021). doi:10.1088/1742-6596/2110/1/012011

26) H. Rofiko, Y. Iriani, and R. Suryana, "Pengaruh Suhu Sintering Pada Pembuatan Strontium Titanat (SrTiO₃) Terhadap Konstanta Dielektrik Menggunakan Metode Co-Precipitation," *Indonesian Journal of Applied Physics,* **7**(1) 28 (2017). DOI: 10.13057/ijap.v7i1.1778

27) D. Nath, F. Singh, and R. Das, "X-ray diffraction analysis by Williamson-Hall, Halder-Wagner and size-strain plot methods of CdSe nanoparticles- a comparative study," *Materials Chemistry and Physics,* **239** 122021 (2020). https://doi.org/10.1016/j.matche mphys.2019.122021

28) O. Bilgili, "The Effects of Mn Doping on the Structural and Optical Properties of ZnO," *Acta Physica Polonica A,* **136**(3) 460-466 (2019).

29) R. K. Chauhan, "Estimation of lattice strain in Mn-doped ZnO nanoparticles and its effect on structural and optical properties," *Indian Journal of Pure & Applied Physics,* **57** 881-890 (2019).

30) I. K. Konstas, and D. Petrakis, "Development of SrTiO₃ Photocatalysts with Visible Light Response Using Amino Acids as Dopant Sources for the Degradation of Organic Pollutants in Aqueous Systems," *Catalysts,* **8**(11) 528 (2018). doi:10.3390/ catal8110528

31) K. Kusdianto, M. Hudandini, D. Jiang, M. Kubo, and M. Shimada, "Effect of Heating Rate on the Photocatalytic Activity of Ag–TiO₂ Nanocomposites by One-Step Process via Aerosol Routes," *Catalysts,* **12**(1) 17 (2021). https://doi.org/10.3390/catal120100 17